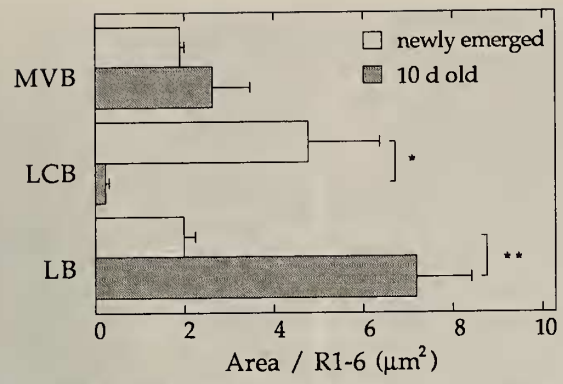

FIG. 4. Areas occupied by multivesicular body (MVB), large complex body (LCB), and lysosomal body (LB) in R1–6. Measurement was done on 23 ommatidia from 5 individuals for each age (n=5). **; $P<0.01$, *; $P<0.05$ (Student's t-test).

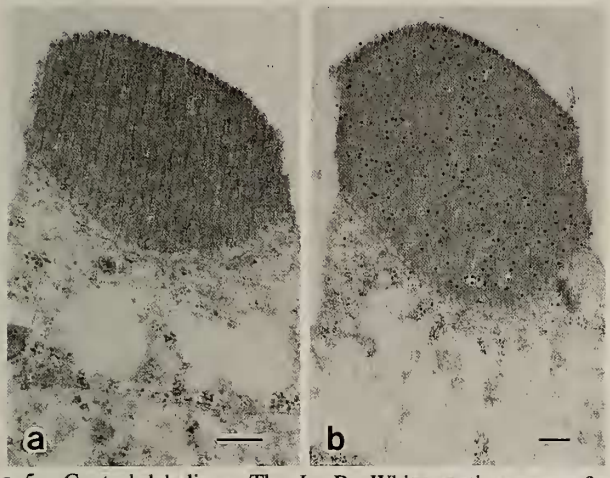

FIG. 5. Control labeling. The L. R. White sections were first labeled either with antiactin (a) or antiopsin (b), and were further treated with the mixture of 15 nm gold-conjugated GAM IgG and 5 nm gold-conjugated GAM IgM. Scale bar=0.2μm.

Figures 6c and d show S1-decorated actin filaments lining the plasma membrane. The actin filaments point away from the rhabdomere (arrowhead triplets): we could not detect any actin filaments with the opposite polarity in this region. The antiactin labeling around the plasma membrane most likely corresponds to these actin filaments (arrows in Fig. 6g). Antiactin also labeled the filaments in the space between the rhabdomere and the cell body (Fig. 6g, h, see also [2]).

DISCUSSION

The results reported here are the following. First, the rhabdomeres of newly emerged flies are developing. These flies are therefore suitable to study the cellular events associated with the rhabdomere morphogenesis. Second, we described opsin-containing large complex body (LCB) in the rER mass. The opsins in the LCB may be incorporated into the rhabdomeres. Finally, electron microscopic histochemistry of opsin and actin suggested that the actin filaments serve as a route for opsin transport towards the rhabdomere.

Double labeling

Two double labeling methods employed here both functioned properly, and gave similar results. The labeling density was consistent except for the antiactin labeling on the rhabdomere in both methods. The observed variation in the density of antiactin labeling is probably attributed to the arrangement of actin in the rhabdomere: actin contributes to the slender core of the microvilli [2, 20]. We cut the hexagonally packed microvilli, each of which is about 100 nm in diameter, roughly along their longitudinal axes. In the ultrathin sections, about 70 nm in thickness, the number of cores contained in a section would vary depending on the cutting angle and/or the degree of distortion of the microvilli arrangement. The number of cores in the section affects the frequency of epitopes exposed on the section surface, which is a determinant of the labeling density.

Opsin synthesis

The photoreceptors of newly emerged flies actively synthesize proteins, which is indicated by the rich content of rER in the cell body (Figs. 1 and 2). The proteins should include opsin, for the rER was occasionally labeled with antiopsin (Fig. 6b, f, Table 1).

The newly emerged flies appeared to have large opsin-bearing structures of irregular profile, which contain vesicles, ribosomes and/or rER, making the cross sectional appearance complex (Figs. 1 and 3). We therefore termed the structure as large complex body (LCB). Some LCBs were enclosed by several layers of membranes densely labeled with antiopsin (Fig. 3f, h). Although some of these resemble autophagic vacuoles, there is also a possibility that the opsins in the LCBs, in the lamellated membranes in particular, are newly synthesized rather than removed from the rhabdomere. Our preliminary observation indicates that the LCBs are abundant even in the late pupal stage and then mostly disappear within two days after emergence: the appearance of the LCBs coincides with the activity of the rhabdomere morphogenesis [15]. The functional significance of the LCBs is remained for further investigation.

MVBs and LBs are both involved in the membrane degradation [8, 11]. Although not frequent, the MVBs and LBs, both contain opsin, were also found in the newly

FIG. 3. Opsin-bearing structures embedded in the rER (arrows) in the photoreceptor cell body. The left column (a,c,e,g) represents the images of conventional EM, whereas the right column (b,d,f,h) represents the L. R. White sections double labeled with antiopsin and antiactin. (a) (b) Multivesicular body. (c) (d) Lysosomal body. (e) (f) Large complex body enclosed by the lamellated membranes (arrowheads). The membranes enclose some rER (arrows). (g) (h) Large complex body without the lamellated membranes. In (h), an LCB enclosed by the lamellated membranes (arrowheads) is also seen. I; intraommatidial space, LB; lysosomal body, M; multivesicular body, R; rhabdomere, r; ribosome, v; vesicles. Scale bar=0.5μm.

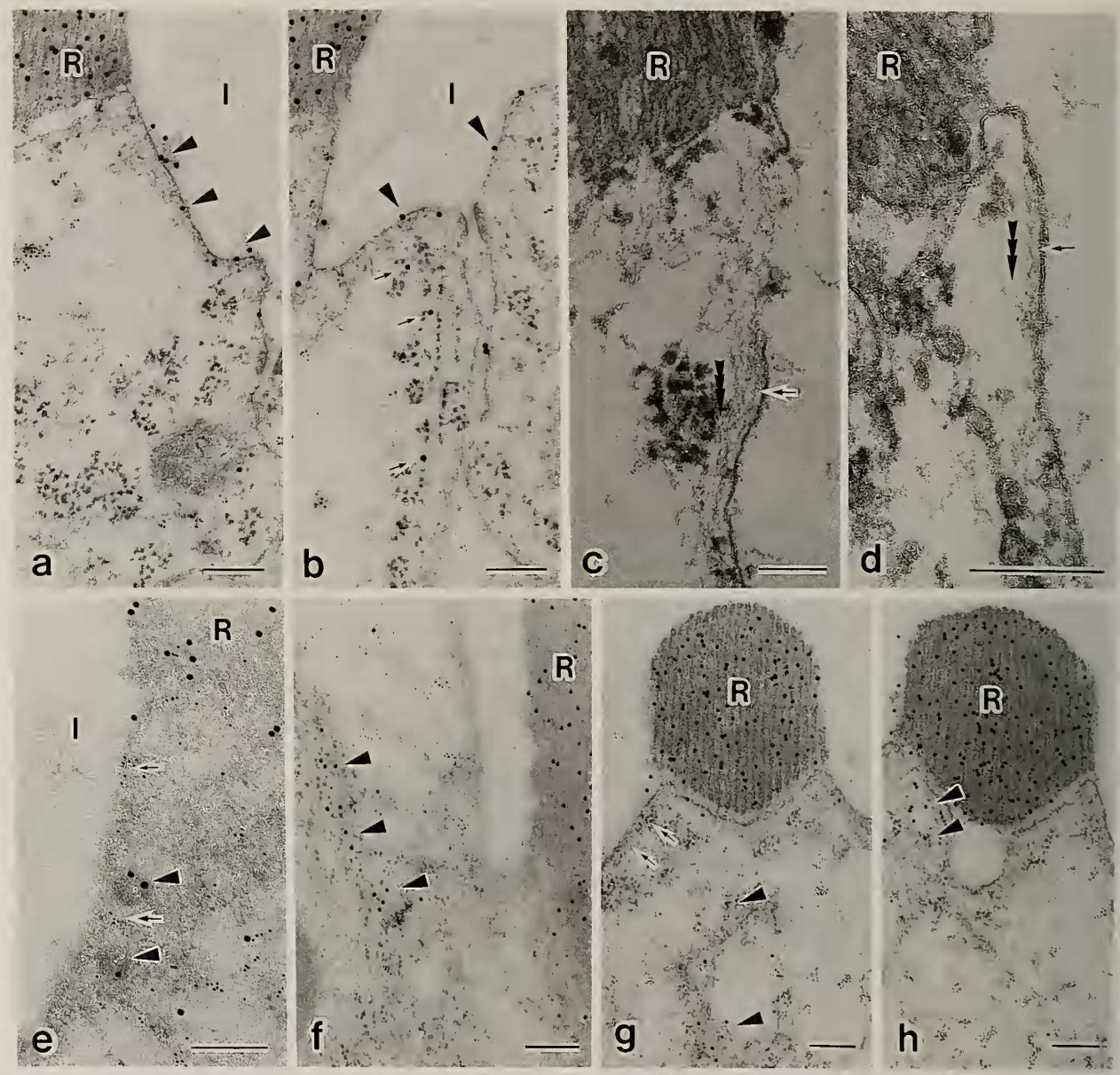

FIG. 6. Histochemistry of opsin and actin in the photoreceptors of newly emerged flies. (a) (b)Antiopsin labeling (arrowheads) on the plasma membrane facing to the intraommatidial space. Arrows in (b) indicate antiopsin labeling on the rER. (c) (d) S1-decorated actin filaments lining the plasma membrane (arrows). The polarity of the filaments was indicated on the left side of the filaments by arrowhead triplets. (e) Opsin-bearing vesicles (arrowheads) found close to the plasma membrane (arrowheads), which was partially lined with antiactin labeling (arrows). (f) Some portions of rER mass were labeled with antiopsin (arrowheads). (g) (h) Antiopsin labeling scattered in the cell body appeared to be associated with some endomembranes (arrowheads). arrows; antiactin labeling. I; intraommatidial space, R; rhabdomere. Scale bar=0.2μm.

emerged flies (Fig. 4), suggesting that the rhabdomere degradation was not inhibited during the stage where the rhabdomere morphogenesis is actively taking place.

Actin and transport of opsin

Transverse sections of the retina clearly show that the photoreceptors have two distinct domains: the rhabdomere and the cell body (Fig. 1). The opsins synthesized in the cell body should be transported to the site of function, the rhabdomere, through the gap between the domains.

There are two possible routes for new opsins to reach the rhabdomere: via the plasma membrane facing to the intraommatidial space [21], and through the subrhabdomeral cisternae (SRC) [14, 24].

Here the antiopsin clearly labeled the plasma membrane (Fig. 6a, b, Table 1). The opsins in the plasma membrane is probably being transported towards the rhabdomere rather than removed from there. One reason for this is that the rhabdomere volume is increasing in this stage (Fig. 2): the flies retain high activity of rhabdomere morphogenesis that

Table 1. Distribution of 15nm gold particles (antiopsin labeling) on the photoreceptors of newly emerged and 10d old flies

	mean particle number±se (%)			
	newly emerged, n=4		10 d old, n=4	
rhabdomere	116.7±18.1	(54.7)	90.1± 8.9	(61.3)
plasma membrane	4.9± 1.0	(2.5)	1.3± 0.1	(0.8)**
MVB	5.6± 2.5	(2.5)	12.1± 1.7	(7.8)
LB	8.4± 4.1	(3.6)	33.1± 2.3	(22.4)
LCB	65.9± 5.4	(33.1)	LCB not found	
other regions	6.4± 1.2	(3.5)	11.2± 1.3	(7.7)
Total	2.7.9±21.4	(100.0)	152.1±11.3	(100.0)

"Other regions" include endomembranes and rER. LCBs were not found in the measured micrographs of 10 d old flies. The particle numbers were compared with the corresponding regions in the different developmental stage. Particle counting was done on 57 photoreceptors (ranging 2–14 photoreceptors per individual) from 4 individuals for each age (n=4).
**; $P<0.05$, Student's *t*-test

should require opsin incorporation into the rhabdomere. Secondly, the labeling density on the plasma membrane is significantly higher in the newly emerged than in 10 d old flies (Table 1). Thirdly, the plasma membrane is lined with the uniformly oriented actin filaments with the plus ends towards the rhabdomere (Fig. 6c, d) and anti-NINAC labeling [13]. As suggested by Adams and Pollard [1] in *Acanthamaeba* myosin I, the myosin-like NINAC could move the membrane-embedded opsin towards the plus end of the actin filaments, i.e., towards the rhabdomere.

In fact, actin is probably involved in the rhabdomere morphogenesis. In a crab, *Hemigrapsus sanguineus*, the rhabdom volume increases at dusk and decreases around dawn [3]. The volume increase was inhibited by treating the isolated eye at dusk with cytochalasin D, which disrupts actin filaments. As the cytochalasin D treatment had no effect at night on the enlarged rhabdom, the inhibition of the volume increase should be attributed not to the disintegration of once established rhabdom but to the disruption of some process(es) in the rhabdom morphogenesis [16]. The most plausible process mediated by the presumptive actin-myosin interaction is the transport of opsin. When applied also at dusk, colchicine, a microtubule inhibitor, failed to stop the volume increase, suggesting that the actin was more directly involved in the rhabdomere morphogenesis than the microtubules [16]. Further analyses using other inhibitory drugs are in progress.

The actin-NINAC interaction also explains another route of opsin transport through the SRC, which is an opsin-containing network that wraps the entire base of the rhabdomere [14, 24]. The SRC is connected to the rER with membrane tubules forming an extensive endomembrane system. The opsins in the SRC are probably originated from the rER, the site of opsin synthesis, through the membrane tubules, although no opsin had been so far localized in the tubules. Here we detected antiopsin labeling in the region between the rhabdomere and the cell body. The labeling appeared to be associated with the vesicles or pieces of membranes (Fig. 6g, h). These endomembranes are most likely parts of the tubules, for the tubules appear in transverse sections as elongated or swollen vesicles [14], or even as fragmented membranes if one side of the tubule was tangentially sectioned. The antiopsin labeling on the rER probably represents new opsins that will be transferred into the tubules (Fig. 6b, f).

The region between the rhabdomere and the cell body is furnished also with the NINAC [13]. By the presumptive interaction between actin and NINAC, the opsins embedded in the endomembranes can be transported towards the rhabdomere.

ACKNOWLEDGMENTS

We thank Dr. T. Tanimura for providing the monoclonal anti-*Drosophila* Rh1 opsin antibody. Drs. T. Tanimura, S. Stowe, and E. Eguchi provided helpful comments in the initial stages of the work. We also thank two anonymous referees for many valuable suggestions on the manuscript. The work was supported by the Grants to K. Arikawa from Whitehall Foundation (Florida, USA), Kihara Foundation for Life Sciences (Yokohama), and the Ministry of Education, Science, and Culture of Japan.

REFERENCES

1 Adams RJ, Pollard TD (1989) Binding of myosin I to membrane lipids. Nature 340: 565–568

2 Arikawa K, Hicks JL, Williams DS (1990) Identification of actin filaments in the rhabdomeral microvilli of *Drosophila* photoreceptors. J Cell Biol 110: 1993–1998

3 Arikawa K, Kawamata K, Suzuki T, Eguchi E (1987) Daily changes of structure, function and rhodopsin content in the compound eye of the crab *Hemigrapsus sanguineus*. J Comp Physiol A 161: 161–174

4 Arikawa K, Williams DS (1989) Organization of actin filaments and immunocolocalization of alpha-actinin in the connect-

ing cilium of rat photoreceptors. J Comp Neurol 288: 640–646

5 Baumann O (1992) Structural interactions of actin filaments and endoplasmic reticulum in honeybee photoreceptor cells. Cell Tissue Res 268: 71–79

6 Besharse JC, Horst CJ (1990) The photoreceptor connecting cilium. A model for the transition zone. In "Ciliary and flagellar membranes" Ed by R. A. Bloodgood, Plenum, New York, pp 389–416

7 Blest AD (1980) Photoreceptor membrane turnover in arthropods: Comparative studies of breakdown processes and their implications. In "The effects of constant light on visual processes" Ed by T. P. Williams and B. N. Baker, Plenum, New York London, pp 217–245

8 Blest AD (1988) The turnover of phototransductive membrane in compound eyes and ocelli. Adv Insect Physiol 20: 1–53

9 Bok D (1985) Retinal photoreceptor-pigment epithelium interactions. Invest Ophthalmol Vis Sci 26: 1659–1694

10 de Couet HG, Tanimura T (1987) Monoclonal antibodies provide evidence that rhodopsin in the outer rhabdomeres of *Drosophila melanogaster* is not glycosylated. Eur J Cell Biol 44: 50–56

11 Eguchi E, Waterman TH (1976) Freeze-etch and histochemical evidence for cycling in crayfish photoreceptor membranes. Cell Tissue Res 169: 419–434

12 Hafner GS, Tokarski TR, Kipp J (1992) Localization of actin in the retina of the crayfish *Procambarus clarkii*. J Neurocytol 21: 94–104

13 Hicks JL, Williams DS (1992) Distribution of myosin I-like *ninaC* proteins in the *Drosophila* retina and ultrastructural analysis of mutant phenotypes. J Cell Sci 101: 247–254

14 Matsumoto-Suzuki E, Hirosawa K, Hotta Y (1989) Structure of the subrhabdomeric cisternae in the photoreceptor cells of *Drosophila melanogaster*. J Neurocytol 18: 87–93

15 Matsushita A, Arikawa K, Eguchi E (1992) Distribution of opsin in the photoreceptors in the late pupal and newly emerged *Drosophila*. Zool Sci 9: 1232

16 Matsushita A, Arikawa K, Eguchi E (1993) Disruption of actin filament organization in the photoreceptors inhibits the rhabdom morphogenesis in a crab *Hemigrapsus*. Zool Sci 10: 86

17 Montell C, Rubin GM (1988) The *Drosophila ninaC* locus encodes two photoreceptor cell specific proteins with domains homologous to protein kinases and the myosin heavy chain head. Cell 52: 755–772

18 Papermaster DS, Schneider BG, Besharse JC (1985) Vesicular transport of newly synthesized opsin from the Golgi apparatus toward the rod outer segment: Ultrastructural immunocytochemical and autoradiographic evidence in *Xenopus* retinas. Invest Ophthalmol Vis Sci 26: 1386–1404

19 Porter JA, Yu MJ, Doberstein SK, Pollard TD, Montell C (1993) Dependence of calmodulin localization in the retina on the NINAC unconventional myosin. Science 262: 1038–1042

20 Saibil HR (1982) An ordered membrane-cytoskeleton network in squid photoreceptor microvilli. J Mol Biol 158: 435–456

21 Schwemer J (1986) Turnover of photoreceptor membrane and visual pigment in invertebrates. In "The molecular mechanism of photoreception" Ed by H Stieve, Springer-Verlag, Berlin Heidelberg New York Tokyo, pp 303–326

22 Stark WS, Sapp R, Schilly D (1988) Rhabdomere turnover and rhodopsin cycle: Maintenance of retinula cells in *Drosophila melanogaster*. J Neurocytol 17: 499–509

23 Stowe S (1980) Rapid synthesis of photoreceptor membrane and assembly of new microvilli in a crab at dusk. Cell Tissue Res 211: 419–440

24 Suzuki E, Hirosawa K (1991) Immunoelectron microscopic study of the opsin distribution in the photoreceptor cells of *Drosophila melanogaster*. J Electron Microsc 40: 187–192

25 Williams DS, Blest AD (1980) Extracellular shedding of photoreceptor membrane in the open rhabdom of a tipulid fly. Cell Tissue Res 205: 423–438

ZOOLOGICAL SCIENCE 11: 399–406 (1994)
© 1994 Zoological Society of Japan

Experimental Perturbations of the *Litonotus-Euplotes* Predator-Prey System

Nicola Ricci and Franco Verni

Dipartimento di Scienze dell'Ambiente e Territorio,
via A. Volta 6 56100 Pisa, Italy

ABSTRACT—A model previously proposed to demonstrate the interactions between *Litonotus* (predator) and *Euplotes* (prey), led to a new round of experiments. The different experimental approaches used to solve these questions (starved cells; killed cells; enzymes; lectins; ions; inhibitors) resulted in quite a new model of the cell interactions which accounts for the different steps of the phenomenon: the main point demonstrated by these experiments is that the cellular cortex of both predator and prey is involved in many of the successive steps of the cascade reactions enabling *Litonotus* to prey upon *Euplotes*

INTRODUCTION

Efforts spent in attempting to deepen our understanding of predation among protozoa are completely justified by the basic importance of the process. Protozoa, indeed, were not only the first primary consumers in the primeval Oceans, but the first predators as well [12]. Such a new trophic niche is quite an important one, due to the two consequences it leads to: (a) it creates new empty spaces for new organisms to settle in, (b) it triggers a sort of evolutionary competition between preys and predators (to escape and to strike each other, respectively) as to their morpho-functional acquisitions. Many examples have been already studied and the knowledge of the *Didinium-Paramecium* [1], *Dileptus-Colpidium* [34], *Enchelys-Tetrahymena* [5], *Chaenea-Uronema* [5]; *Homalozoon-Paramecium* [4] predator-prey systems, cannot but help us to complete our overall picture of this phenomenon considered from a more specific sinecological point of view: in this perspective, indeed, the study of predator-prey interactions also lends itself to be used in an attempt to penetrate the adaptive strategies, conditioning the reciprocal (co)evolution of predators and preys. Let us recall the example of the bat-moth relationships, as a truly paradigmatic one, to clarify our idea [28].

In this context we studied another predatory model, namely that of *Litonotus lamella-Euplotes crassus*, focusing our attention successively on (a) the ultrastructure of the toxicysts of the predators [11], (b) the ultrastructural analysis of the consequences to *Euplotes* of toxicyst discharge by *Litonotus* [32]; (c) the peculiar digestion process [33] and, finally, (d) the behavioural patterns following each other along a path characterised by the succession of several basic steps, namely casual encounter (CE); toxicyst discharge (TD); research (R); engulfment of the prey (PE)[8]. The predator-prey interaction model proposed in the previous paper focused our attention on several closely related problems, which represented the targets of the next round of experiments: (a) how is the toxicyst-discharging system triggered and controlled? (b) which are the spatio-temporal sequences of a toxicyst-discharge phenomenon?

The unique nature of our pet-organism protozoa (i.e. indeed perfect eukaryotic cells and complete organisms, at the same time) offers a double advantage: (a) it enables us to use all those techniques typical of experimental studies on cell interactions to investigate also the relationships between entire organisms and (b) it allows us to transfer any results obtained for these truly sophisticate organisms to the general field of cell biology.

MATERIALS AND METHODS

Both *L. lamella* and *E. crassus* were grown, collected and used as already described by Ricci and Verni [24]. The observations were made with a Wild M5 (20–60X) stereomicroscope, and a Leitz Orthoplan (400X) microscope (together with its Nomarsky interferential contrast), coupled to a Panasonic TVC camera and a VHS videorecorder. Unless otherwise indicated, the prey organism was *E. crassus*. The following specific procedures were followed for the different kinds of experiments:

Expt. 1 The effects of starvation on preys and on predators were studied using normal and starved *Litonotus*, exposed to both normal and starved *Euplotes*. Normal populations of predators were used 4 days after the last feeding, while the starved ones were tested after 11 days. Normal *Euplotes* were not fed for 24 hr, while the starved ones were used 7 days after the last feeding.

Expt. 2 To study the role played by the body itself, of both the predator and the prey, in the specific toxicyst discharge (TD) processes at the very moment when the two organisms come into direct contact with each other and the TD itself is triggered and actually occurs, both *Litonotus* and *E. crassus* were frozen, and then thawed at room temperature (the experimental populations were immersed in liquid nitrogen for 2 min): in this way the structurally and chemically preserved, but physically inert bodies of both *Litonotus* and *Euplotes* were tested with living prey or predator respectively. In some of these experiments homogenized *Euplotes* were also used.

Expt. 3 Whenever a predator contacts a prey TD occurs: does TD affect the microenviroment where it occurred? How far for TD area is such an effect perceived? How long does it persist? How is the behaviour of *Euplotes* affected? To solve these problems, many TD

Accepted May 31, 1994
Received December 16, 1993

events were videorecorded and the videotapes scored frame by frame according to the standard technique for behavioural studies reported elsewere by Ricci [20]. In this way we quantified: a) the subcircular area where the TD effects are perceived by *Euplotes*; b) their duration; c) the changes in behaviour of the prey.

Expt. 4 To assess the role possibly played by calcium concentration in the sea water, 3 different standard set ups (cf. Expt. 5) were prepared: the first contained standard marine water (control), the second 15 mM calcium chloride, the third the same concentration of $CaCl_2$ plus 0.1 mM EDTA, to inhibit the effects of the calcium. Previous experiments, carried out with 5, 10, 15, 20, and 25 mM Ca^{++} and with 0.01, 0.1 and 10 mM EDTA had shown that the best results were obtained with 15 mM Ca^{++} and with 0.1 mM EDTA. In other words these two concentrations were the lowest capable of inducing clearcut results. Five experiments were then carried out and microvideorecorded, to measure: (a) the time lag between the introduction of *Litonotus* and the first instance of TD (this period of time will be referred to as TD Δt throughout this paper, it somehow measures the efficiency to *Litonotus* in intercepting the prey); (b) the time lag between the introduction of *Litonotus* and the actual engulfment of the killed prey (this period of time will be referred to as I Δt in this paper, it somehow measures the efficiency of *Litonotus* feeding on the prey); (c) the length of the backward motion of *Litonotus* following TD; (d) the number of TD per *Litonotus*.

Expt. 5 The effects of trypsin (Sigma, T8253; concentration 2.5, 2, 1.5, 1 and 0.5%) were also studied. About 50 *Litonotus* were incubated in the different concentration for various time periods (15, 30, 60, 90, 120, 180, 210 and 240 min); they were washed 3 times and then used in a 50 μl droplet with concentrated *Euplotes*, to study the TD Δt, I Δt and the percentage of inhibited (namely not-toxicyst discharging) *Litonotus*. When 100% TD inhibition was induced, the *Litonotus* still incubated by trypsin were washed free of the enzyme fresh water and then used in *Euplotes* populations to monitor their recovery period.

Expt. 6-A The effects of concanavalin-A (Con-A, Sigma C2010; concentration 2, 1.5, 1, 0.5 and 0.25%; treatment time 15, 30, 60, 90, 120, 150, 180 and 210 min) on *Litonotus* were studied by washing the treated cells after different periods of time and measuring TD Δt, I Δt and the percentage of inhibited cells, when these experimental *Litonotus* were transferred into a 50 μl droplet of concentrated preys. The same treatments were also carried out on incubating *Litonotus* in the same dosages of Con-A and for the same times as before, in the presence of 40 mM of α-methyl-D-mannoside, well-known as a specific competitor of Con-A. The same parameters were measured.

Expt. 6-B Concentrations of 2 and 1% of Con-A were also used to incubate *Euplotes* for 15, 30, 60, 90, 120, 150, 180, 210, 270, 330, and 390 min: these populations were washed three times and then exposed to *Litonotus*, to measure the TD Δt, the I Δt, the percentage of non-discharging *Litonotus*.

Expt. 7 In a final experimental approach, *Litonotus* was treated with different concentrations (0.5, 0.25, 0.125, 0.06, 0.03 and 0.015%) of cycloheximide (Chx)(Sigma C-6255) for different times (1 to 9 hr); they were used singly with populations of *Euplotes* to measure TD Δt, IΔt and the percentage of TD inhibition. When 100% TD inhibition was obtained the still incubated cells were washed free of Chx and then used with *Euplotes* to study the kinetics of their recovery in terms of the percentage of TD inhibited cells.

RESULTS

Expt. 1 The effects of different starvation of *Litonotus* and *Euplotes*.

Previous microscope observations (Verni, unpublished results) had shown that the longer the starvation, the more caudal the distribution of toxicysts: the effects were statistically significant. On the basis of these findings, the consequences of starvation were studied more specifically.

The results obtained in this round of experiments demonstrated that (a) severe starvation affects the efficiency of predator's TD: Table 1, the III and the IV columns vs the I and the II; (b) the starvation of the preys affects, to a limited extent, the ingestion capability of *Litonotus* (Table 1, IΔt, the II vs the I column and the IV column vs the III), while it does not affect the corresponding TD Δt.

Expt. 2 The predatory interactions between *Litonotus* and frozen-thawed *Euplotes*.

Litonotus cannot be frozen and then thawed, without being disrupted: no result could be obtained, except that the area where a disrupted *Litonotus* lies is avoided by the preys. Normal *Litonotus* exposed to a population of frozen-thawed *Euplotes* demonstrated that: (a) *Litonotus* can ingest them without discharging any toxicysts (Fig. 1B); (b)IΔt is longer than twice as much as that of the control (Fig. 1: B vs A); (c) when freshly prepared homogenate of *Euplotes* is added to the system, ID Δt is strikingly reduced (Fig. 1C).

Expt. 3 The TD-affected area.

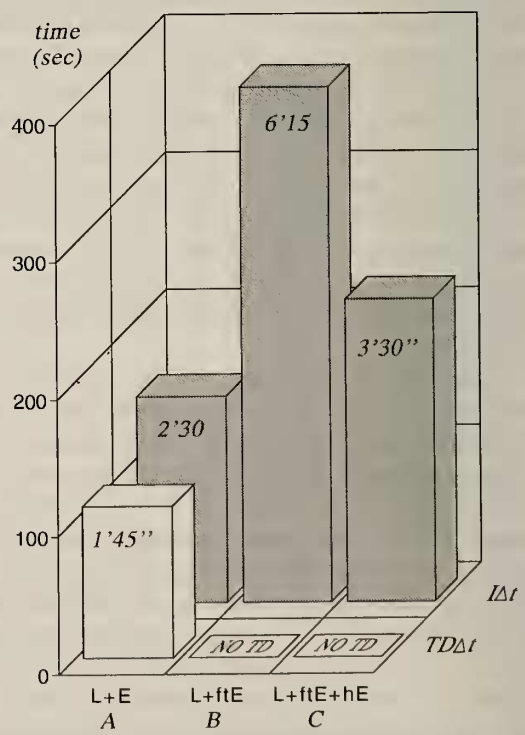

Fig. 1. The TDΔt (white bars) and the IΔt (shadowed bars) of *Litonotus* (L) in presence of [A] normal *Euplotes* (E), [B] frozen-thawed *Euplotes* (ftE) and [C] ftE and homogenated *Euplotes* (hE). On the ordinates the times in seconds are reported.

TABLE 1. The effects of starvation, on the predation of *Litonotus lamella* on *Euplotes crassus*, measured by the durations of the TDΔt and of the IΔt (described in Materials and Methods section).

		normal **Litonotus**		starved **Litonotus**	
		+ normal **Euplotes**	+ starved **Euplotes**	+ normal **Euplotes**	+ starved **Euplotes**
TDΔt	$\bar{x}$	**1'25"**	**1'20"**	**2'21"**	**2'15"**
	s	55"	50"	1'12	1'18"
	n	35	26	29	32
IΔt	$\bar{x}$	**2'30"**	**3'**	**3'42"**	**4'9"**
	s	1'	1'5"	1'15"	1'18"
	n	35	26	29	32

FIG. 2. The temporal trend of avoidance of the "toxic" area by *Euplotes*, expressed in terms of individuals (ordinate: %) creeping away from it, in the time (abscissa: sec). The shadowed bars show the same trend of *Euplotes* avoiding frozen-thawed *Litonotus*

The results we obtained are the following: (a) the effects of a TD event extend around the TD point over a sub-circular area of about 300μm in diameter, (b) the same effects increase up to their maximum for 90 sec after the TD event and last for about 3 min; (c) the behaviour of the preys is clearly affected by the TD event as demonstrated by the high frequency of avoidances induced in *Euplotes* by TD immediately afterwards (Fig. 2, shadowed areas); the avoidances correspond to the behavioural pattern called Side Stepping Reaction [19] and indicated as SSR; (d) these SSR occur according to a temporal pattern parallel to that of *Euplotes* avoiding the area where a frozen-thawed disrupted *Litonotus* is placed (Fig. 2, white areas).

TABLE 2. The effects of Ca^{++} (15 mM) on the 4 parameters indicated on the left; BM = the length of the backward motion of a *Litonotus lamella* after discharging its toxicysts: it is measured in Relative Units (RU): 1 RU = 1 species-specific length of *Litonotus lamella* $\simeq$250μm. The number of observations for each parameter was of 50

populations / parameters studied	Control	15 mM Ca^{++}	15 mM Ca^{++} & 0.1 mM EDTA
TDΔt (sec)	43±17	41.5±18	42±26
BM (RU)	1.1±0.7	2.5±0.7	1.2±0.6
IΔt (sec)	132±30	186±80	139±33
n^0 of TD per *Litonotus*	1.2±0.4	2.4±0.5	1.2±0.5

Expt. 4 The role of Ca^{++} in the environment.

The results given in Table 2 clearly show that calcium ions affect the general physiology of the *Litonotus-Euplotes* system at least at three different levels: (a) TD Δt is not affected; (b) the length of the backward motion is doubled; (c) IΔt increases by about 50%; (d) the number of TD per *Litonotus* is doubled. EDTA inhibits calcium effects, as expected. As considered in the Materials and Methods section, the differential effects of calcium ions on TD Δt (no effect) and on IΔt (strong inhibition), actually demonstrate the importance of both parameters in interpreting correctly the effects of calcium ions on the *Litonotus-Euplotes* system.

Expt. 5 The effect of trypsin on *Litonotus*

The enzyme was already known to affect the physiology of *Litonotus*; progressively higher concentrations and longer treatments, indeed, induce (a) a progressive darkening of the cytoplasm, (b) a rounding of the body shape, (c) reduced locomotion, (d) immobilization and (e) lysis of the cell (Ricci and Verni, unpublished results). It was found (Fig. 3) that the different concentrations used for the different times indicated in Material and Methods, clearly affect TD Δt (the higher the concentration, the longer TD Δt) but not IΔt (the difference between TD Δt and IΔt is indeed rather constant). For a certain concentration a longer treatment affects the percentage of cells not discharging their toxicysts (Fig. 4), while TD Δt tends to be more or less constant, the different values depending solely upon trypsin concentration. Once

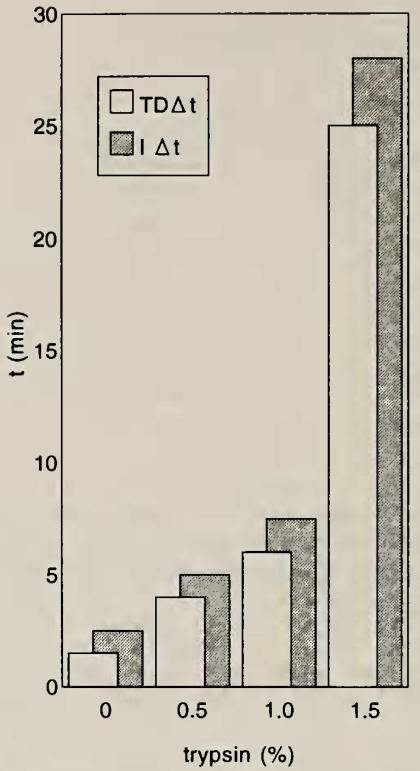

FIG. 3. The average TDΔt and IΔt induced by the concentrations of trypsin, given on the abscissa; 0% of trypsin=controls

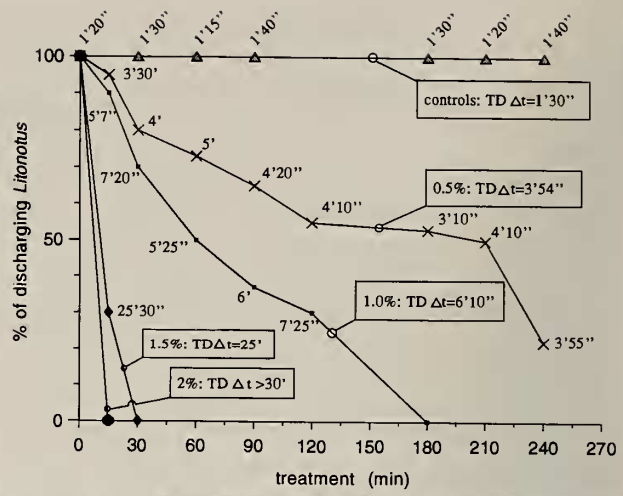

FIG. 4. The progressive action of the trypsin in the time: for a certain concentration the longer the treatment (abscissa) the smaller the percentage of discharging *Litonotus*. The figure close to each of the different points along the curves, represents the average TDΔt observed for that point; the figures in the small panels represent the trypsin concentration for the different curves and the relative mean values of the TDΔt.

100% inhibition is induced (namely, when no *Litonotus* can discharge its toxicysts) they still behave quite normally and their physiology seems to be unaffected: after washing, these completely inhibited populations recover 80% of their TD activity within 30–60 min, and 100% of their potentialities within 60–120 min.

Similar treatments with trypsin were also conducted on *Euplotes*; the enzyme either has no effect al all on both TD Δt or IΔt, and it kills the preys.

Expt. 6A The effects of Con-A on *Litonotus*.

The results of the experiments are the following: (a) the higher the Con-A concentration, the stronger the effect, on TD Δt, but not on IΔt (Table 3) (b) for the same concentration, the longer the treatment, the stronger the effect on TD Δt but not on IΔt (Table 3) (c) as the Con-A concentration

TABLE 3. The TDΔt and the IΔt of different populations of *Litonotus* treated by different concentrations of Con A (shown in the first line) for different times, given in the left column

t \ Con A		2%		1.5%		1%		0.5%		0.25%		control	
		TDΔt	IΔt	TDΔt	IΔt	TDΔt	IΔt	TDΔt	IΔt	TDΔt	IΔt	TDΔt	IΔt
	n	15	15	10	10	10	10	10	10			8	8
15'	$\bar{x}$	>30'	>35'	3'	4'	2'	3'20'	1'31"	2'20"	ND	ND	2'	3'
	s	—	—	1'20"	1'46"	50"	1'30"	1'	1'17"			1'05"	1'25"
	n	**14**	**14**	**14**	**14**	**12**	**12**	**11**	**11**	**12**	**12**	**8**	**8**
30'	$\bar{x}$	>30'	>35'	10'50"	15'30"	6'23"	7'30"	2'10"	3'30"	2'15"	3'24"	1'20"	2'30"
	s	—	—	2'19"	3'	3'55"	3'27"	1'	1'27"	1'	1'21"	1	1'50'
	n			**16**	**16**	**9**	**9**	**10**	**10**	**11**	**11**	**8**	**8**
60'	$\bar{x}$	†	†	>30	>35'	8'10"	11'50"	5'20"	7'	2'27"	3'40"	1'30"	2'55"
	s			—	—	5'15"	5'	2'20"	2'	1'12"	1'25"	1'15"	1'20"
	n					**10**	**10**	**7**	**7**			**8**	**8**
90'	$\bar{x}$			†	†	11'15"	13'30"	10'35"	12'15"	ND	ND	2'10"	3'15"
	s					5'18"	7'47"	2'20"	2'30"			050"	1'35"
	n					**18**	**18**	**13**	**13**			**8**	**8**
120'	$\bar{x}$					>30'	>35'	12'35"	13'43"	ND	ND	1'20"	2'20"
	s					—	—	1'24"	1'21"			1'05"	1'50"
	n							**6**	**6**	**10**	**10**	**8**	**8**
150'	$\bar{x}$					†	†	12'40"	13'26"	5'	6'42"	1'50"	3'
	s							1'25"	1'10"	1'36"	1'40"	1'10"	1'50"